Multiphase Organization Is a Second Phase Transition Within Multi-Component Biomolecular Condensates

Konstantinos Mazarakos[a] *and Huan-Xiang Zhou*[a,b,]*

[a]Department of Physics and [b]Department of Chemistry, University of Illinois at Chicago, Chicago, IL 60607, United State

AUTHOR INFORMATION

Corresponding Author

* E-mail: hzhou43@uic.edu

ABSTRACT. We present a mean-field theory for the multiphase organization of multi-component biomolecular condensates and validate the theory by molecular dynamics simulations of model mixtures. A first phase transition results in the separation of the dense phase from the bulk phase. In a second phase transition, the components in the dense phase demix to localize in separate regions that attach to each other. The second phase transition occurs when the strength of cross-species attraction goes below the mean strength of the self-attraction of the individual species and reaches a critical value. At a given strength of cross-species attraction, both of the phase transitions can be observed by decreasing temperature, leading first to phase separation and then to demixing of the dense phase. The theory and simulations establish the disparity in strength between self and cross-species attraction as a main driver for the multiphase organization of multi-component biomolecular condensates.

TOC GRAPHICS

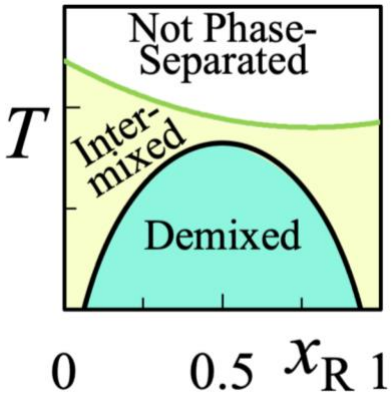

KEYWORDS phase separation; mean-field theory; critical temperature; demixing; cross-species attraction.

Biomolecular condensates, formed via liquid-liquid phase separation, mediate a myriad of cellular functions, including ribosome preassembly and mRNA sequestration under stress.[1-2] Instead of a single homogeneous dense phase, multi-component condensates, both inside cells and reconstituted using purified components, show multiphase organization.[1, 3-11] Multiphase coexistence has also been observed in coarse-grained molecular simulations.[8, 11-16] Yet the theoretical underpinning is still unclear. Here we present a simple theoretical model to show that the multiphase organization of multi-component condensates is a second phase transition. Whereas the first phase transition that leads to the separation of condensates from the bulk phase is driven by overall attraction among the macromolecular components,[17] the second phase transition, leading to multiphase organization within condensates, is driven by disparity in strength between self and cross-species attraction.

Our model systems have two components, D and R, which are either spherical particles or chains of such particles. The particles attract each other, with interaction energy $-\varepsilon_{\alpha\beta}$ between species α and β (= D or R) at contact and 0 otherwise. The strengths, $\varepsilon_{\mathrm{DD}}$ and $\varepsilon_{\mathrm{RR}}$, of self-attraction of the two components, are different. Specifically, $\varepsilon_{\mathrm{DD}} > \varepsilon_{\mathrm{RR}}$, so that the critical temperature for phase separation of pure D is higher than the counterpart of pure R. The phase separation of a mixture is driven by the self-attraction of D (for "driver") but regulated by the self-attraction of R (for "regulator") and the cross-species attraction between D and R.[14, 18-19] We work in temperatures (T) below the critical temperature, T_{c}, for the phase separation of the mixture, where the first phase transition has resulted in the coexistence of a dense phase and a bulk phase. Our interest is the dense phase, specifically its multiphase organization.

Let us first consider the case where the components are particles. In a mean-field treatment, the Helmholtz free energy, F, of the dense phase has an enthalpic contribution, due to pairwise interactions of the particles, and an entropic contribution, due to mixing of the species:

$$F = U - TS_{\mathrm{mix}} \quad [1]$$

The enthalpic contribution can be obtained by enumerating the three kinds of contact pairs, DD, RR, and DR:

$$U = -\varepsilon_{\mathrm{DD}}N_{\mathrm{DD}} - \varepsilon_{\mathrm{RR}}N_{\mathrm{RR}} - \varepsilon_{\mathrm{DR}}N_{\mathrm{DR}} \quad [2]$$

where $N_{\alpha\beta}$ denotes the total number of contact pairs between species α and β. Let the total number of all contact pairs be N_{p}:

$$N_{\mathrm{DD}} + N_{\mathrm{RR}} + N_{\mathrm{DR}} = N_{\mathrm{p}} \quad [3]$$

Note that N_{p} is proportional to the total number, M, of particles:

$$N_{\mathrm{p}} = \frac{c}{2}M \quad [4]$$

where c represents the average number of contact pairs formed by a particular particle.

Both the partition of N_{p} among the three kinds of contact pairs and the mixing entropy depend on the organization of the dense phase. Consider first the demixed state, where D and R form separate dense phases. We have

$$N_{\mathrm{DR}} = 0 \quad [5a]$$

and

$$\frac{N_{\mathrm{RR}}}{N_{\mathrm{DD}}} = \frac{x_{\mathrm{R}}}{1 - x_{\mathrm{R}}} \quad [5b]$$

where x_{R} is the mole fraction of the regulator species. Solving eqs [3], [5a], and [5b], we find

$$\text{Demixed: } \begin{cases} N_{\mathrm{DD}} = (1 - x_{\mathrm{R}})N_{\mathrm{p}} \\ N_{\mathrm{RR}} = x_{\mathrm{R}}N_{\mathrm{p}} \\ N_{\mathrm{DR}} = 0 \end{cases} \quad [5c]$$

In the intermixed state, D and R form a single homogeneous dense phase. Around a given D particle, the chance of a contact partner being an R particle or another D particle is proportional to the mole fraction of the partner species. Thus

$$\frac{N_{\mathrm{DD}}}{N_{\mathrm{DR}}} = \frac{1}{2}\frac{1 - x_{\mathrm{R}}}{x_{\mathrm{R}}} \quad [6a]$$

where the factor of one half accounts for the fact that DR pairs can be obtained in two ways: either D is the center and R is a contact partner, or R is the center and D is the contact partner. Likewise we have

$$\frac{N_{\mathrm{RR}}}{N_{\mathrm{DR}}} = \frac{1}{2}\frac{x_{\mathrm{R}}}{1 - x_{\mathrm{R}}} \quad [6b]$$

Solving eqs [3], [6a], and [6b], we find

$$\text{Intermixed: } \begin{cases} N_{\mathrm{DD}} = (1 - x_{\mathrm{R}})^2 N_{\mathrm{p}} \\ N_{\mathrm{RR}} = x_{\mathrm{R}}^2 N_{\mathrm{p}} \\ N_{\mathrm{DR}} = 2x_{\mathrm{R}}(1 - x_{\mathrm{R}})N_{\mathrm{p}} \end{cases} \quad [6c]$$

In the demixed state, by definition, the mixing entropy is 0,

$$\text{Demixed: } S_{\mathrm{mix}} = 0 \quad [7]$$

for any x_{R}. Intermixing gives rise to a mixing entropy

$$\text{Intermixed: } \frac{S_{\mathrm{mix}}}{Mk_{\mathrm{B}}} = -(1 - x_{\mathrm{R}})\ln(1 - x_{\mathrm{R}}) - x_{\mathrm{R}}\ln x_{\mathrm{R}} \quad [8]$$

The change in F from the intermixed to the demixed state is finally found as[17]

$$\frac{\Delta F}{Mk_{\mathrm{B}}T} = \chi x_{\mathrm{R}}(1 - x_{\mathrm{R}}) - (1 - x_{\mathrm{R}})\ln(1 - x_{\mathrm{R}}) - x_{\mathrm{R}}\ln x_{\mathrm{R}} \quad [9]$$

where

$$\chi = \frac{c}{k_B T}\left(\varepsilon_{DR} - \frac{\varepsilon_{DD} + \varepsilon_{RR}}{2}\right) \quad [10]$$

Decreasing χ, e.g., by weakening the cross-species attraction, favors the demixed state. When χ is decreased to a critical value,

$$\chi_{\odot} = -2 \quad [11a]$$

the demixed state becomes the thermodynamically stable state for the first time, at $x_R = 0.5$. If ε_{DD}, ε_{RR}, and T are fixed, the critical value for ε_{DR} is

$$\varepsilon_{DR\odot} = \frac{\varepsilon_{DD} + \varepsilon_{RR}}{2} - \frac{2}{c} k_B T \quad [11b]$$

Note that $\varepsilon_{DR\odot}$ is below the mean of ε_{DD} and ε_{RR}, and the gap grows with increasing temperature. When $\varepsilon_{DR} < \varepsilon_{DR\odot}$, the demixed state becomes stable (relative to the intermixed state) over a range of x_R around 0.5 (Fig. 1). For example, at $\varepsilon_{DR} = \varepsilon_{DR\odot} - 0.1 k_B T/c$, the stable x_R range of the demixed state is (0.315, 0.685). On the borders of this x_R range, the intermixed and demixed states are equally stable and hence they coexist. The relation between ε_{DR} and the two border x_R values is a binodal. If instead we fix ε_{DR} (below the mean of ε_{DD} and ε_{RR}) and vary T, we obtain a critical temperature for demixing:

$$T_{\odot} = \frac{c}{2k_B}\left(\frac{\varepsilon_{DD} + \varepsilon_{RR}}{2} - \varepsilon_{DR}\right) \quad [12]$$

When $T < T_{\odot}$, there is a range of x_R values, centered at x_R = 0.5, in which the demixed state is stable. The relation between T and the two border x_R values is another type of binodal.

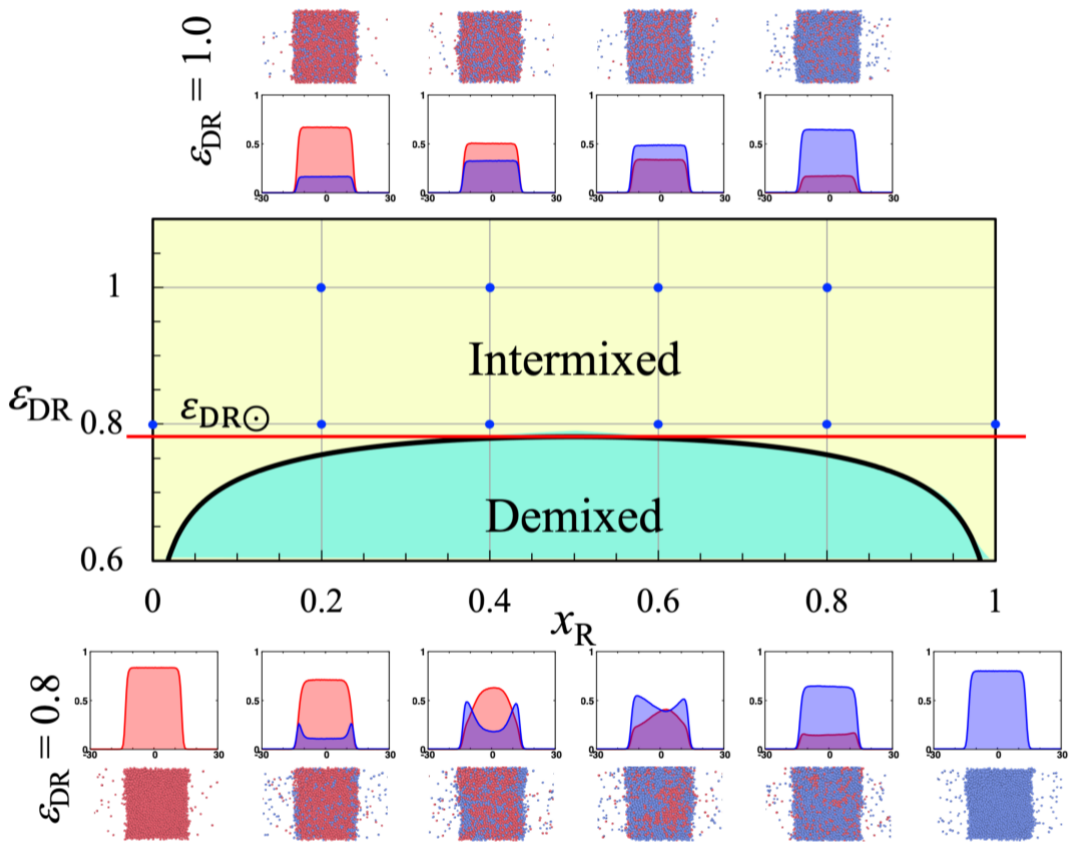

Figure 1. The ε_{DR} vs. x_R binodal of particle mixtures predicted by the mean-field theory. The binodal separates the intermixed zone (yellow) from the demixed zone (cyan). The critical value for ε_{DR} is shown by a red horizontal line. Density profiles of the two species (D: red; R: blue) and representative snapshots of particle mixtures obtained in molecular dynamics simulations are shown for the indicated ε_{DR} and x_R values.

The above free energy calculation can be easily extended to polymer blends, where each polymer is a chain of particles. For a binary blend, with both component the same chain length L (representing the number of particles per chain), the free energy of the dense phase is[20-21]

$$\frac{\Delta F}{Mk_BT} = \chi x_R(1-x_R) - \frac{(1-x_R)}{L}\ln(1-x_R) - \frac{x_R}{L}\ln x_R \qquad [13]$$

where the mixing entropy is reduced due to chain connectivity. The critical χ value for demixing is now

$$\chi_{\odot} = -\frac{2}{L} \qquad [14a]$$

Chain connectivity thus reduces the magnitude of $\chi_{\odot}$. The corresponding critical value for $\varepsilon_{\mathrm{DR}}$ is

$$\varepsilon_{\mathrm{DR}\odot} = \frac{\varepsilon_{\mathrm{DD}} + \varepsilon_{\mathrm{RR}}}{2} - \frac{2}{cL} k_{\mathrm{B}} T \qquad [14b]$$

A comparison between eqs [11b] and [14b] shows that the gap between $\varepsilon_{\mathrm{DR}\odot}$ and the mean of $\varepsilon_{\mathrm{DD}}$ and $\varepsilon_{\mathrm{RR}}$ is narrower for chain mixtures than for particle mixtures. The critical temperature for chain mixtures is

$$T_{\odot} = \frac{cL}{2k_{\mathrm{B}}} \left(\frac{\varepsilon_{\mathrm{DD}} + \varepsilon_{\mathrm{RR}}}{2} - \varepsilon_{\mathrm{DR}} \right) \qquad [15]$$

which is higher than the counterpart (eq [12]) for particle mixtures. The higher critical values of $\varepsilon_{\mathrm{DR}}$ and temperature mean that demixing occurs more easily in chain mixtures than in particle mixtures.

This mean-field theory makes a number of important predictions on the organization of the dense phase of mixtures formed by phase separation. First, when the strength ($\varepsilon_{\mathrm{DR}}$) of the cross-species attraction decreases below the mean strength of the self-attraction of the individual species and reaches a critical value $\varepsilon_{\mathrm{DR}\odot}$, a second phase transition occurs within the dense phase, resulting in demixing of the species. Second, the second phase transition occurs at a higher $\varepsilon_{\mathrm{DR}}$ for chain mixtures than for particle mixtures. Third, when $\varepsilon_{\mathrm{DR}}$ is below the critical value $\varepsilon_{\mathrm{DR}\odot}$, there is a range of mixing ratios, centered at equimolar mixing (i.e., $x_{\mathrm{R}} = 0.5$), where demixing occurs. This means that demixing most readily occurs when the species are mixed at equimolarity. Fourth, when $\varepsilon_{\mathrm{DR}}$ is below the mean of $\varepsilon_{\mathrm{DD}}$ and $\varepsilon_{\mathrm{RR}}$, there is a critical temperature $T_{\odot}$. Demixing occurs only when T is below $T_{\odot}$. All these predictions are consistent with our initial results of demixing from molecular dynamics simulations of binary mixtures of Lennard-Jones particles or chains of such particles (L =10).[14] For these Lennard-Jones systems, we used $\varepsilon_{\alpha\beta}$ to denote the well-depth for the interaction potential energy between particles of species α and β (= D or R), and fixed $\varepsilon_{\mathrm{DD}}$ and $\varepsilon_{\mathrm{RR}}$ at 1 and 0.9, respectively. Complete intermixing between D and R was observed at $\varepsilon_{\mathrm{DR}}$ = 1.2 and 1.0, but demixing was observed at $\varepsilon_{\mathrm{DR}}$ = 0.8 for chain mixtures at lower temperatures. We thus suspected that demixing was driven by the disparity between cross-species interaction

strength ε_{DR} and the self-interaction strengths ε_{DD} and ε_{RR}. This suspicion is now justified by the mean-field theory. We now reexamine the simulation results on the demixing of the Lennard-Jones systems in light of the mean-field theory. Demixing slows down the equilibration process and also can produce multiple metastable states. We thus extended the simulations here from 10 million to 100 million steps (ref [14]; Fig. S1) and carried out five replicate runs when there were signs of demixing.

In Fig. 1, we display the density profiles and representative snapshots of the particle mixtures at k_BT = 0.65, along with the ε_{DR} vs. x_R binodal predicted by the mean-field theory. As already noted, at $\varepsilon_{DR} \geq 1.0$, only the intermixed state was observed, as indicated by uniform densities of the components inside the dense phase. At ε_{DR} = 0.8, there was local enrichment of the regulator (i.e., lower-T_c) species at the interface between the dense and bulk phases, which we attribute at least partly to the finite size of the simulation systems and does not necessarily indicate the demixed state per se. With c = 7.7, eq [11b] predicts $\varepsilon_{DR\odot}$ = 0.78, which is consistent with the absence of demixing in the simulations at ε_{DR} = 0.8. The mean-field theory further predicts demixing at ε_{DR} = 0.6 for all x_R values except those near 0 or 1, which are in agreement with simulations (not shown).

We display the corresponding results for chain mixtures at k_BT = 1.7 in Fig. 2. Again, only intermixing was observed at ε_{DR} = 1.0, but now there was clear indication of demixing at ε_{DR} = 0.8 for $0.2 \leq x_R \leq 0.8$. These observations are consistent with the mean-field theory, which predicts $\varepsilon_{DR\odot}$ = 0.84 (eq [14b] with cL = 31) and demixing for $0.105 \leq x_R \leq 0.895$ at ε_{DR} = 0.8. At x_R = 0.2 and 0.4, the dense phase in the simulations consisted of a D-rich region at the center, bordered by two R-rich regions on the two sides ("R-D-R" configuration; bottom rows in Figs. 2 and S2A,B). At x_R = 0.6, the dense phase had the R-D-R configuration in two of the five replicate runs but a "D-R" configuration in the other three runs, where a D-rich region and an R-rich region attach to each other (bottom row in Figs. 2 and S2C). At x_R = 0.8, the D chains in the dense phase coalesce into a cylinder, located near the interface with the bulk phase (bottom row in Figs. 2 and S2D).

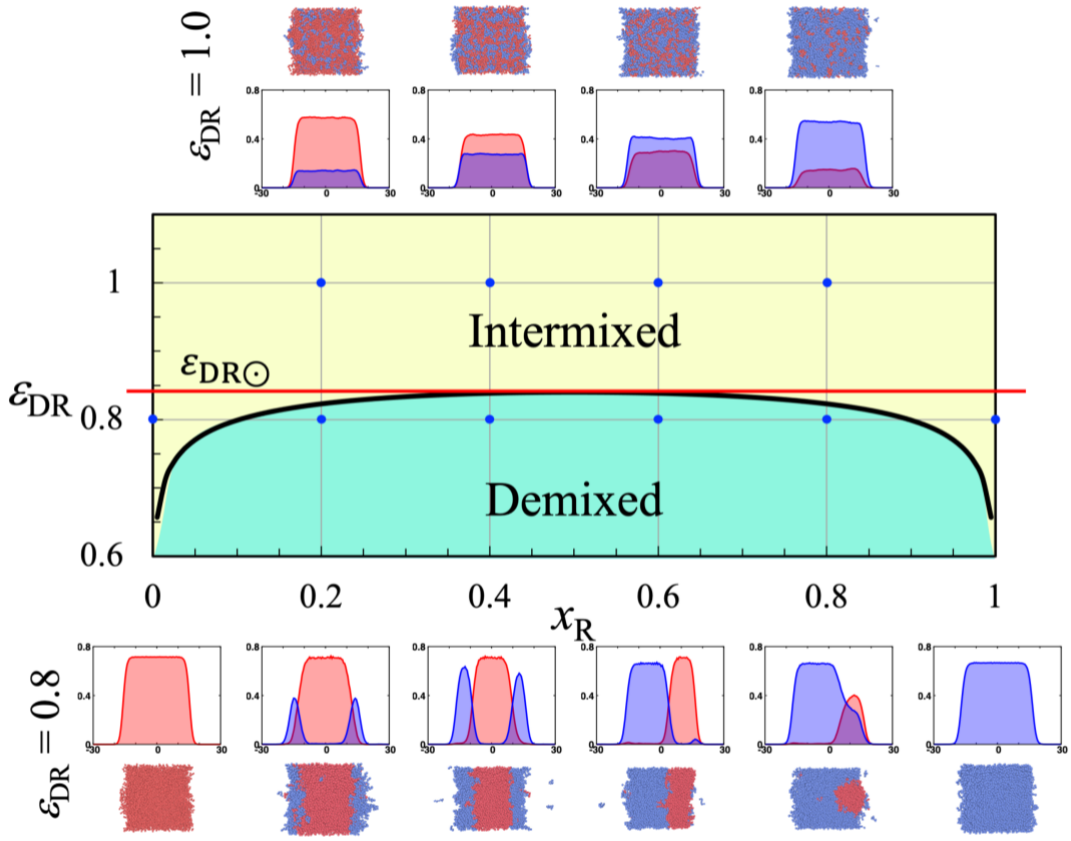

Figure 2. The ε_{DR} vs. x_R binodal of chain mixtures predicted by the mean-field theory. The binodal separates the intermixed zone (yellow) from the demixed zone (cyan). The critical value for ε_{DR} is shown by a red horizontal line. Density profiles of the two species (D: red; R: blue) and representative snapshots of chain mixtures obtained in molecular dynamics simulations are shown for the indicated ε_{DR} and x_R values.

Next we consider the effects of temperature on the behaviors of the dense phase of chain mixtures at $\varepsilon_{DR} = 0.8$. Figure 3 displays the T vs. x_R binodal predicted by the mean-field theory, with a critical temperature of $k_B T_\odot = 2.325$ for demixing. It should be noted that there is also a critical temperature, T_c, for phase separation (i.e., the first phase transition). The $k_B T_c$ values have a parabolic dependence on x_R, with a minimum of 2.403 at $x_R = 0.78$ (green curve in Fig. 3).[14] The entire T vs. x_R plane can be divided into three distinct zones. Above the T_c curve, there is no phase separation; between the T_c curve and the T vs. x_R binodal, the dense phase is a homogenous mixture of the components; below the T vs. x_R binodal, the dense phase is in a demixed state. As already noted when presenting Fig. 2, when $k_B T = 1.7$, the chain mixtures with $x_R = 0.2$, 0.4, 0.6,

and 0.8 all fell into the demixed zone. In contrast, when $k_BT = 2.3$, these mixtures all fell into the intermixed zone (top row in Fig. 3). At this temperature, the two species were well-mixed in the dense phase, although for $x_R = 0.2$ and 0.4 there was local enrichment of R chains at the interface between the dense and bulk phases, which we again attribute to the finite size of the simulation systems.

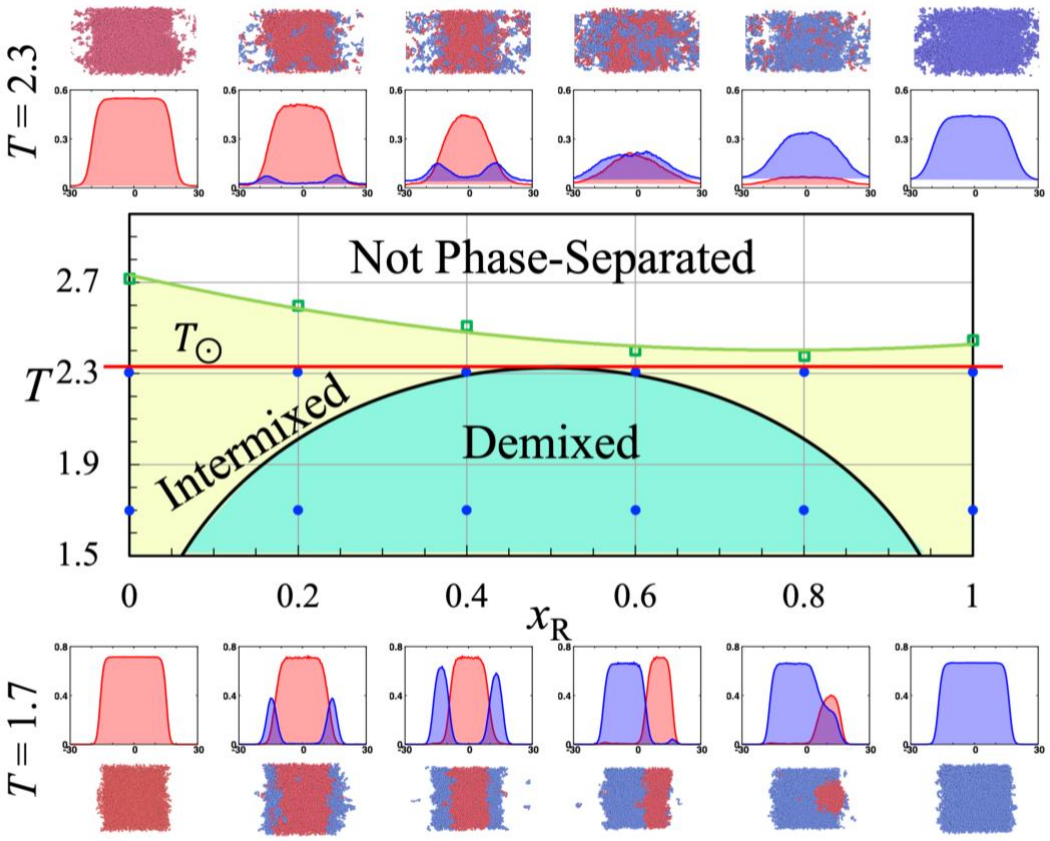

Figure 3. The T vs. x_R binodal of chain mixtures predicted by the mean-field theory. The binodal (black curve) separates the intermixed zone (yellow) from the demixed zone (cyan). The T_c curve (green) further separates the intermixed zone from the non-phase-separated zone (white). A red horizontal line is drawn at $T = T_\odot$ (in units of $1/k_B$). Density profiles of the two species (D: red; R: blue) and representative snapshots of chain mixtures obtained in molecular dynamics simulations are shown for the indicated T and x_R values.

Lastly let us look at the transition from the demixed state to the intermixed state at a fixed x_R as k_BT increased from 1.7 to 2.3 (Figs. 4 and S2). For x_R = 0.2 and 0.4, with increasing temperature, more and more R chains migrated from the outer R-rich regions to the central D-rich

region, leading to the merge of the R-rich regions, while D chains migrated in the reverse direction. The same scenario applied to the R-D-R configuration at $x_R = 0.6$ when k_BT changed from 1.7 to 2.3. For the D-R configuration at $x_R = 0.6$ and $k_BT = 1.7$, with increasing temperature, D-chains and R-chains migrated toward each other, ultimately leading to the complete mixing of the two species. For $x_R = 0.8$, as k_BT changed from 1.7 to 2.0, more and more D-chains in the cylinder migrated into the R-rich region, while R-chains spread into a wider region. When k_BT reached 2.1, the two species were already well-mixed.

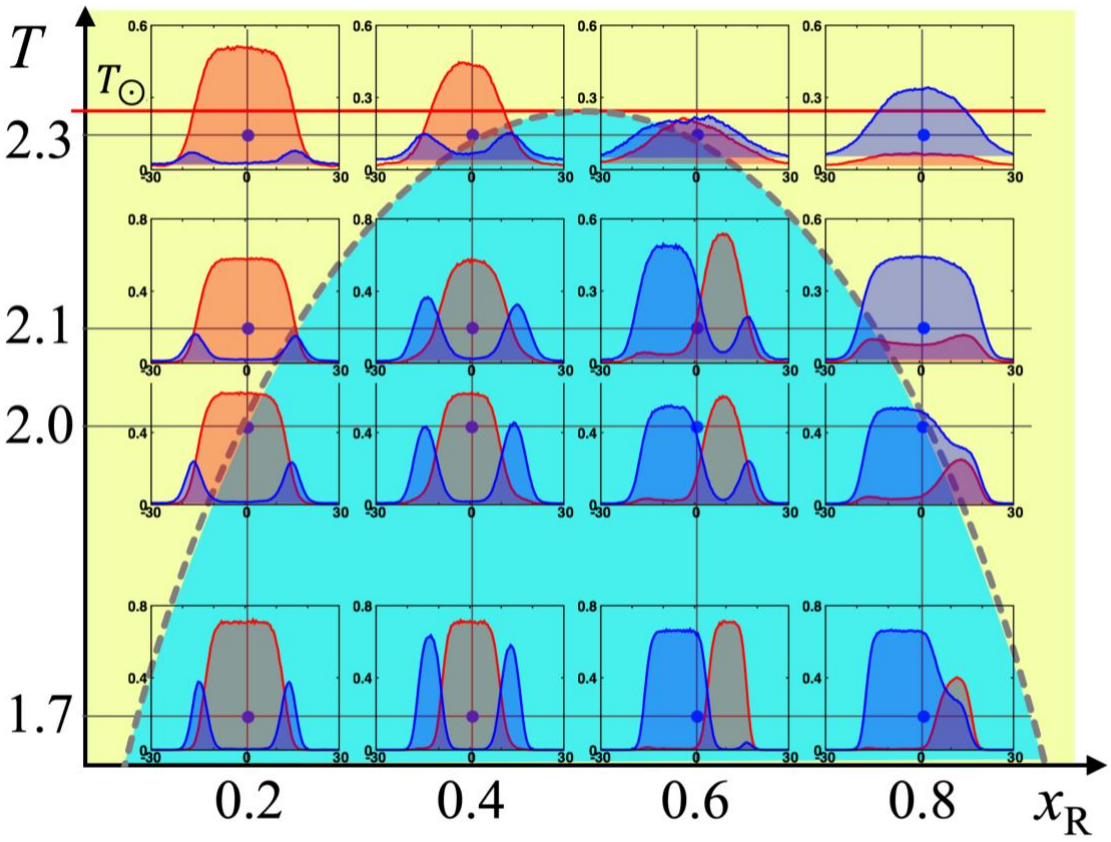

Figure 4. Detailed view into an area spanning k_BT from 1.7 to 2.3 and x_R from 0.2 to 0.8, showing the transition from the demixed at $k_BT = 1.7$ to the intermixed state at $k_BT = 2.3$. Density profiles of the two species (D: red; R: blue) and representative snapshots of chain mixtures obtained in molecular dynamics simulations are shown for various combinations of T and x_R values.

In conclusion, we have presented a mean-field theory that demonstrates that the multiphase reorganization in the dense phase of mixtures is a second phase transition, after the first phase

transition resulting in separation of the dense phase from the bulk phase. Molecular dynamics simulations of model mixtures have provided crucial test of the theory, including the existence of a critical value for the strength of cross-species attraction and a critical temperature for demixing. At a given strength of cross-species attraction, both of the phase transitions can be observed by decreasing temperature, leading first to phase separation and then to demixing of the dense phase. The theory and simulations establish the disparity in strength between self and cross-species attraction as a main driver for multiphase organization, and provide a much needed conceptual framework for understanding the complex phase behaviors of bimolecular condensates.

ASSOCIATED CONTENT

Supporting Information. The following file is available free of charge.

Two supporting figures: illustrating the procedure of the molecular dynamics simulations; showing an expanded version of Fig. 4, with results from five replications for each (T, x_{R}) combination (PDF)

AUTHOR INFORMATION

Notes

The authors declare no competing financial interests.

ACKNOWLEDGMENT

This work was supported by National Institutes of Health Grant GM118091.

REFERENCES

1. Feric, M.; Vaidya, N.; Harmon, T. S.; Mitrea, D. M.; Zhu, L.; Richardson, T. M.; Kriwacki, R. W.; Pappu, R. V.; Brangwynne, C. P. Coexisting Liquid Phases Underlie Nucleolar Subcompartments. *Cell* **2016,** *165*, 1686-1697.

2. Mateju, D.; Franzmann, T. M.; Patel, A.; Kopach, A.; Boczek, E. E.; Maharana, S.; Lee, H. O.; Carra, S.; Hyman, A. A.; Alberti, S. An Aberrant Phase Transition of Stress Granules Triggered by Misfolded Protein and Prevented by Chaperone Function. *EMBO J.* **2017,** *36*, 1669-1687.

3. Jain, S.; Wheeler, J. R.; Walters, R. W.; Agrawal, A.; Barsic, A.; Parker, R. ATPase-Modulated Stress Granules Contain a Diverse Proteome and Substructure. *Cell* **2016,** *164*, 487-498.

4. West, J. A.; Mito, M.; Kurosaka, S.; Takumi, T.; Tanegashima, C.; Chujo, T.; Yanaka, K.; Kingston, R. E.; Hirose, T.; Bond, C., et al. Structural, Super-Resolution Microscopy Analysis of Paraspeckle Nuclear Body Organization. *J Cell Biol* **2016,** *214*, 817-830.

5. Fei, J.; Jadaliha, M.; Harmon, T. S.; Li, I. T. S.; Hua, B.; Hao, Q.; Holehouse, A. S.; Reyer, M.; Sun, Q.; Freier, S. M., et al. Quantitative Analysis of Multilayer Organization of Proteins and RNA in Nuclear Speckles at Super Resolution. *J. Cell. Sci.* **2017,** *130*, 4180-4192.

6. Boeynaems, S.; Holehouse, A. S.; Weinhardt, V.; Kovacs, D.; Van Lindt, J.; Larabell, C.; Bosch, L. V. D.; Das, R.; Tompa, P. S.; Pappu, R. V., et al. Spontaneous Driving Forces Give Rise to Protein−RNA Condensates with Coexisting Phases and Complex Material Properties. *Proc. Natl. Acad. Sci. USA* **2019,** *116*, 7889-7898.

7. Putnam, A.; Cassani, M.; Smith, J.; Seydoux, G. A Gel Phase Promotes Condensation of Liquid P Granules in *Caenorhabditis elegans* Embryos. *Nat Struct Mol Biol* **2019,** *26*, 220-226.

8. Alshareedah, I.; Moosa, M. M.; Raju, M.; Potoyan, D. A.; Banerjee, P. R. Phase Transition of RNA-Protein Complexes into Ordered Hollow Condensates. *Proc. Natl. Acad. Sci. USA* **2020,** *117*, 15650-15658.

9. Ghosh, A.; Zhang, X.; Zhou, H. X. Tug of War between Condensate Phases in a Minimal Macromolecular System. *J. Am. Chem. Soc.* **2020,** *142*, 8848-8861.

10. Sanders, D. W.; Kedersha, N.; Lee, D. S. W.; Strom, A. R.; Drake, V.; Riback, J. A.; Bracha, D.; Eeftens, J. M.; Iwanicki, A.; Wang, A., et al. Competing Protein-RNA Interaction Networks Control Multiphase Intracellular Organization. *Cell* **2020,** *181*, 306-324.

11. Kaur, T.; Raju, M.; Alshareedah, I.; Davis, R. B.; Potoyan, D. A.; Banerjee, P. R. Sequence-Encoded and Composition-Dependent Protein-RNA Interactions Control Multiphasic Condensate Morphologies. *Nat. Commun.* **2021,** *12*, 872.

12. Harmon, T. S.; Holehouse, A. S.; Pappu, R. V. Differential Solvation of Intrinsically Disordered Linkers Drives the Formation of Spatially Organized Droplets in Ternary Systems of Linear Multivalent Proteins. *New J. Phys.* **2018,** *20*, 045002.

13. Regy, R. M.; Dignon, G. L.; Zheng, W.; Kim, Y. C.; Mittal, J. Sequence Dependent Phase Separation of Protein-Polynucleotide Mixtures Elucidated Using Molecular Simulations. *Nucleic Acids Res* **2020,** *48*, 12593-12603.

14. Mazarakos, K.; Zhou, H. X. Macromolecular Regulators Have Matching Effects on the Phase Equilibrium and Interfacial Tension of Biomolecular Condensates. *Protein Sci.* **2021,** *30*, 1360-1370.

15. Pal, T.; Wessen, J.; Das, S.; Chan, H. S. Subcompartmentalization of Polyampholyte Species in Organelle-Like Condensates Is Promoted by Charge-Pattern Mismatch and Strong Excluded-Volume Interaction. *Phys Rev E* **2021,** *103*, 042406.

16. Sanchez-Burgos, I.; Espinosa, J. R.; Joseph, J. A.; Collepardo-Guevara, R. Valency and Binding Affinity Variations Can Regulate the Multilayered Organization of Protein Condensates with Many Components. *Biomolecules* **2021,** *11*, 278.

17. Zhou, H. X.; Nguemaha, V.; Mazarakos, K.; Qin, S. Why Do Disordered and Structured Proteins Behave Differently in Phase Separation? *Trends Biochem. Sci.* **2018,** *43*, 499-516.

18. Nguemaha, V.; Zhou, H. X. Liquid-Liquid Phase Separation of Patchy Particles Illuminates Diverse Effects of Regulatory Components on Protein Droplet Formation. *Sci. Rep.* **2018,** *8*, 6728.

19. Ghosh, A.; Mazarakos, K.; Zhou, H. X. Three Archetypical Classes of Macromolecular Regulators of Protein Liquid-Liquid Phase Separation. *Proc. Natl. Acad. Sci. USA* **2019,** *116*, 19474-19483.

20. Flory, P. J. Thermodynamics of High Polymer Solutions. *J. Chem. Phys.* **1941,** *9*, 660-661.

21. Huggins, M. L. Solutions of Long Chain Compounds. *J. Chem. Phys.* **1941,** *9*, 440-440.